Heat Generation and Neutron Beam Characteristics in A High Power Pulsed Neutron Source*

Dong W. Jerng and John M. Carpenter
Intense Pulsed Neutron Source
Argonne National Laboratory
Argonne, Illinois 60439, U.S. A.

Abstract

As an effort for the conceptual design of a high power pulsed spallation source, a Monte Carlo model was developed for heat generation and neutronics studies. In this paper, we present two sets of our calculation results. The first set of calculation was performed with a simple target model to investigate general characteristics of power distribution and neutron production with various proton energies ranging from 0.8 to 12 GeV. The second set of calculation was performed with a more realistic target model including major components of the target system to provide basic parameters for engineering design of the high power pulsed spallation source. Calculation results generally confirms that higher proton energy provides an advantage in target cooling system requirements and yet lower neutron beam intensity as a counter effect.

1. Introduction

The pulsed spallation neutron source under the present study consists of two targets split by a vaccume region in-between called flux trap and six moderators. The proton beam is at 1 MW time-averaged power with the proposed proton energy of 2.2 GeV. It is intended to deliver five times higher neutron flux than any currently operating facility in the world. The power distributions and the neutron beam characteristics in such a high power pulsed neutron source are main results of this paper. Although 2.2 GeV is the proposed energy of protons for the high power spallation source currently under consideration, a calculation with 9 GeV protons was also performed for the investigation of the effects of extremely high proton energies on the heat load and neutron utilization. Also, a series of calculation was performed to provide an insight to the relationship between impinging proton energy and the distribution of power and neutrons using an idealized target system. This calculation also served as a benchmark for the validation of the code system and physical models used in the Monte Carlo method.

As a computing tool for the Monte Carlo calculations, the LAHET code system was used. The LAHET code system has been developed in Los Alamos National Laboratory (LANL) and mainly consists of an LANL version of the high energy transport code (LAHET) and the general Monte Carlo code for neutron and photon transport (MCNP) with several associated codes [1]. LAHET calculates high energy particle cascades and transports including neutrons above 20 MeV. For the intranuclear cascade calculation in LAHET, the Bertini model has been used which is generally recognized as acceptable up to the particle energy of 3.5 GeV. For the transport calculation of neutrons below 20 MeV and photons, MCNP has been used.

A validation of the LAHET code system and physical model was performed for two parameters which were of most interests for our objectives: the energy deposition in the target and the neutron production rate. For the validation, the target was modeled as 20 disks of 5 cm thickness and 10 cm diameter with 2 mm gaps between disks for water coolant. The target was housed by stainless steel structure imbedded in the beryllium reflector. The proton beam was assumed of a gaussian distribution truncated at 4 cm in radius with the full-width-at-half-maximum (FWHM) radius of 2 cm. The target length was enough to encompass the stopping

* Work sponsored by the U.S. Department of Energy

length of energetic protons and tantalum was assumed for the target material. Fig. 1 shows the calculated ratio of energy deposition in the target to the proton beam energy. Considering the small difference in mass and nuclear composition between lead and tantalum, it is concluded that Fig. 1 confirms the validity of the LAHET code system and physical models used in the calculation. Fig. 2 shows the neutron production rate in the tantalum target compared with that in the lead target. It is seen that the neutron production rate is a little higher with tantalum than with lead. However, it is again concluded that the computer code and physical models set up for this study are sound enough for the next stage calculation.

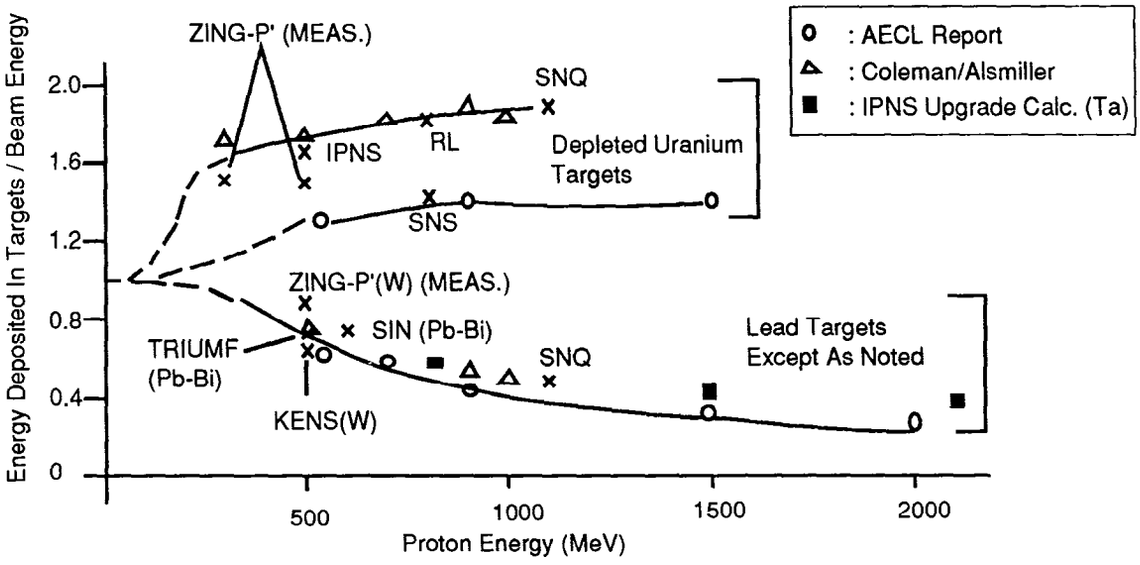

Fig.1 A validation of IPNS Upgrade calculation model - heat deposition in targets (Source for other than IPNS upgrade calculation : Reference 2)

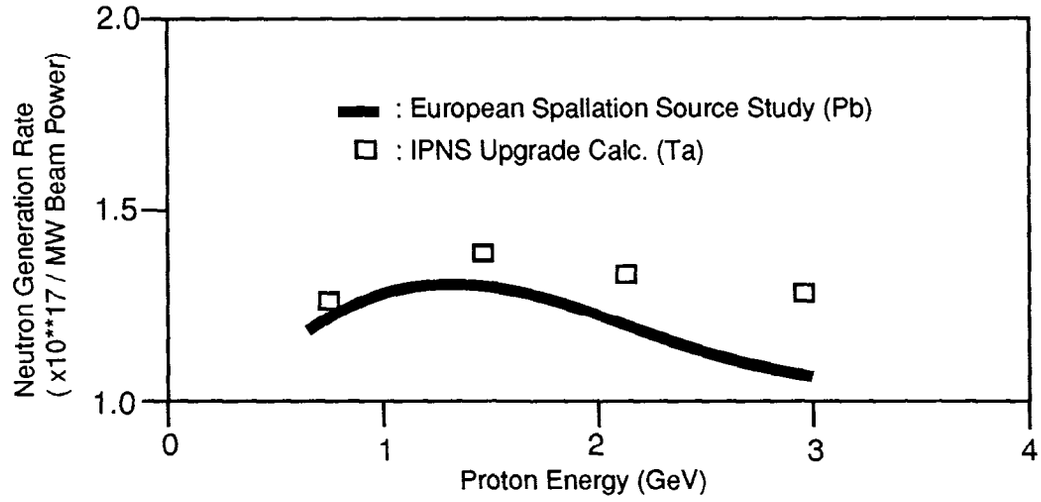

Fig.2 A validation of IPNS Upgrade calculation model - neutron generation rate (Source for European Spallation Source Study : Reference 3)

2. Heat Deposition and Neutron Production with Various Proton Energies

Although the hardron cascade model incorporated in LAHET is recommended for the proton energy up to 3.5 GeV, we calculated power density and neutron current distributions with several proton energies up to 12 GeV. The target model and proton beam conditions used in this series of calculation was the same as used for the code validation except that the target length was prolonged to 2 m for the calculations with 6 and 12 GeV protons. The calculation results are summarized in Table 1 and Figs. 3 and 4 show the spatial distributions of power density and neutron currents. As expected, higher proton energy yields higher neutron production per proton but the neutron production rate normalized to 1 MW proton beam is found to be peaked at 1.5 GeV and slowly decrease as proton energy increases. The maximum current and power density are observed to be proportional to each other although the location of the maximum power density occurs at the first disk and that of the maximum current occurs at the second disk as seen in Figs.3 and 4 respectively. The total power deposited in the target is found to be almost constant, i.e. between 60 to 70 % of beam power as long as the target dimension is sufficiently large enough to accommodate the slow-down of cascade particles. The fluctuation of the power density and neutron current near the end of target shown in Figs.3 and 4 are due to the statistical uncertainty of the Monte Carlo calculation, since the fewer particles remain at the deeper location in the target.

Table 1. Calculation summary (based on 1-MW Beam except neutron yields)

Proton energy	Neutron yield per proton	Neutron production rate ($x10^{17}$n/sec)	Maximum current [a] ($x10^{14}$ n/cm^2 /sec)	Maximum power density [b] (kW/cm^3)	Total power deposition in the target (MW)
0.8 GeV	16.3	1.28	2.0	0.604	0.692
1.5 GeV	33.6	1.41	1.90	0.477	0.627
2.2 GeV	48.8	1.39	1.80	0.439	0.619
3.0 GeV	64.4	1.34	1.65	0.415	0.626
6.0 GeV	115.6	1.20	1.39	0.371	0.654
12.0 GeV	194.8	1.01	1.25	0.307	0.656

a neutron current at the cylindrical surface (radius: 6.2 cm) of the target housing
b power density over a disk (radius: 5 cm and thickness :5 cm) of the target

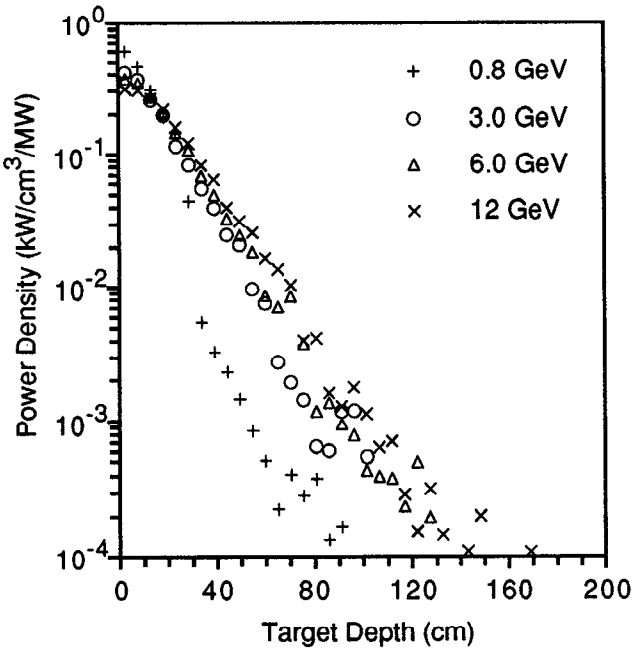

Fig 3. Power density along the target depth

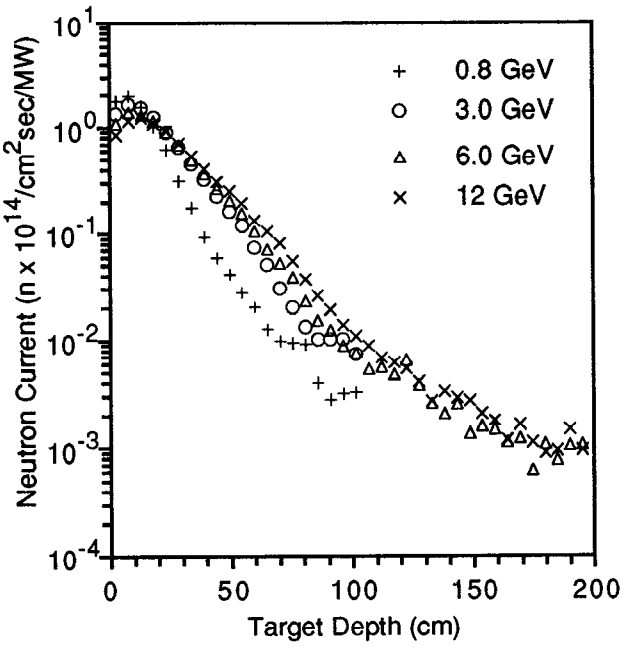

Fig 4. Neutron current along the target depth

3. High Power Target Station Model

The target station including targets, moderators, and neutron beam lines were modeled with a reflector and shield surrounding these components. Geometrical and material features of key components modeled for Monte Carlo simulation are listed in Table 2. An isometric view of the target and moderators is shown in Fig. 5 and the labels for six moderators are indicated also in Fig.5. Fig.6 shows a plan view of the target station from the top for the illustration of neutron beam lines. The moderators and neutron beam lines are covered by the boron decoupler to cut off the thermal neutron scattered into the beam lines from the reflector. There are three neutron beam lines from each moderator totaling 18 beam lines in the target station. The beam lines are separated by an angle of 15°. Fig.7 shows the arrangements of the reflector, shield and removable assemblies for remote handling systems. All calculations are based on proton beam with a gaussian distribution of 2.5 cm FWHM radius and 5 cm radius truncated conditions. The calculation results in subsequent sections are normalized results based on 1 MW proton beam in time average.

Table 2. Geometrical and material features of the key target station components

Component	Geometry and Dimension	Material
Target	split targets : four elliptic disks [a] in the1st target nine elliptic disks [a] in the 2nd target	tantalum
Housing	rectangle with rounded side surfaces 18 cm wide, 12 cm high, and 12 cm long (1st target housing) and 40 cm long (2nd target housing) with a spring at the back	0.5 cm thick stainless steel
Flux Trap	18 cm long section between the housings	vacuum
Coolant	coolant channel gap between target disks : 0.2 cm	water
Moderator	1st target moderators: 5 cm x10 cm x 10 cm flux trap moderators: 5 cm x10 cm x 20 cm 2nd target moderators: 10 cm x 10 cm x 10 cm	water
Boron Decoupler	2 cm thick clad surrounding moderators and neutron beam lines except the beam line face	natural boron with 3.3 % of normal density [b]
Reflector	cylinder of r = 54 cm, h = 100 cm	beryllium
Shield	annulus of r_i = 54 cm, r_o = 100 cm, h = 100 cm	iron

[a] minor radius = 5.5 cm, major radius = 7.5 cm, thickness = 2.5 cm (1st target), 3.5 cm (2nd target)

[b] boron density for the decoupling energy of 1.0 eV and 1/e reduction of neutron flux cross the decoupler.

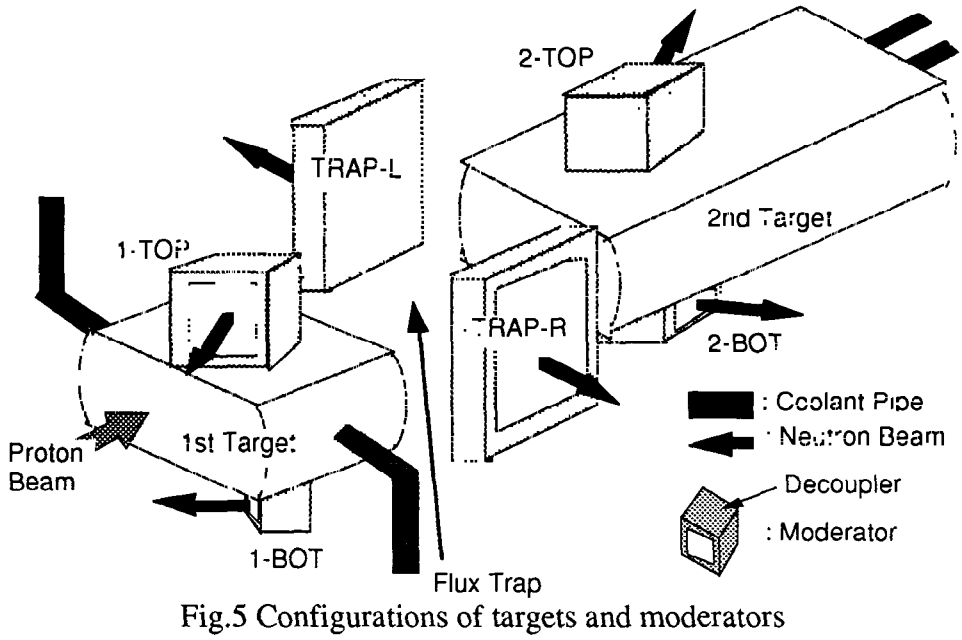

Fig.5 Configurations of targets and moderators

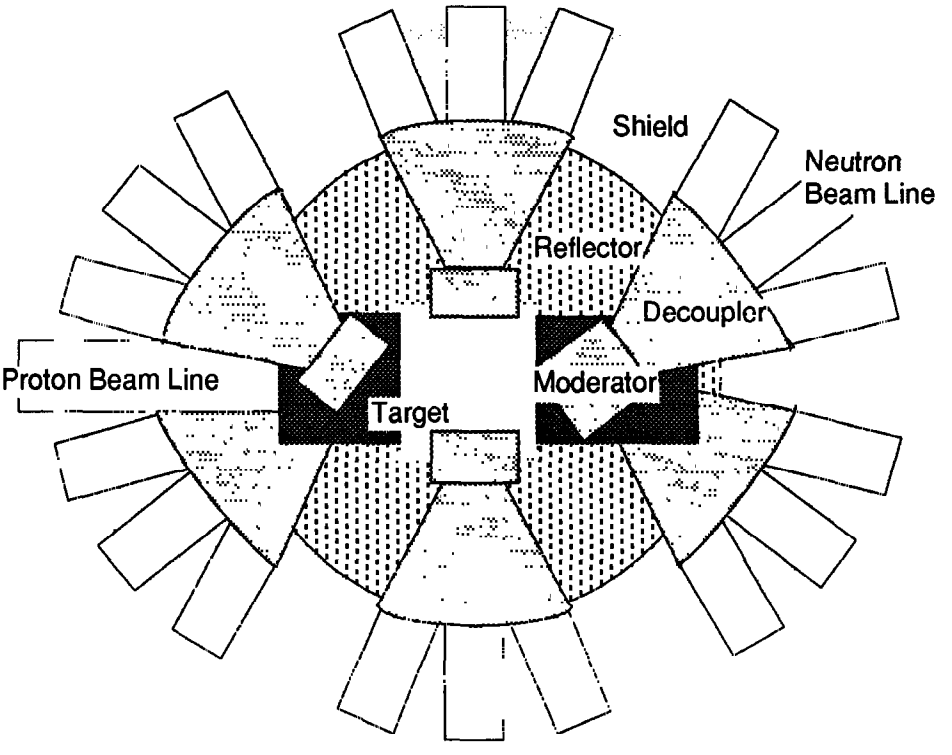

Fig.6 Arrangement of neutron beam lines

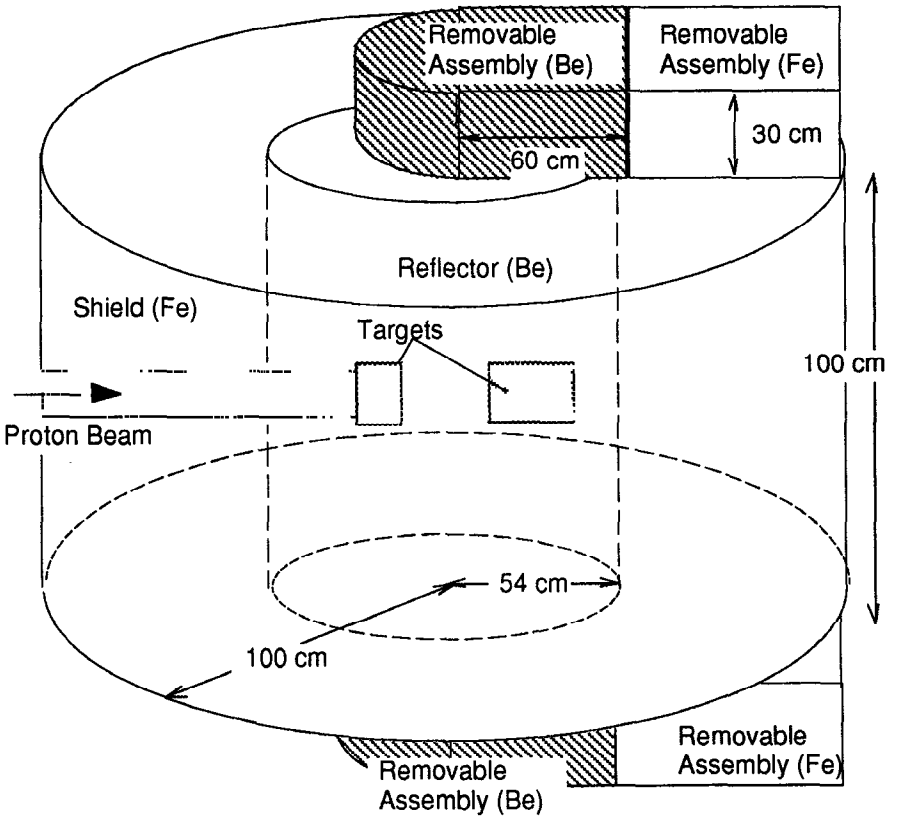

Fig.7 Schematic of the systems surrounding the targets

4. Power Distribution in the Target Station

The power distribution in the target station is summarized in Table 3. With 2.2 GeV protons, about 90 % of the beam power is deposited in the target station and the 10 % is thought either to be absorbed in the form of binding energy resulting from the change of isotope compositions during the cascade process or to escape through neutron and photon leak. For instance, the neutrons escaping from the system in the model is about 9.7 neutrons/proton. Assuming 8 MeV for the neutron binding energy, this leak constitutes about 35 kW/MW-beam. Thus, the overall energy balance is thought to be satisfied in the calculation. The overall energy balance was also confirmed in the case of 9 GeV protons. In this case, about 95 % of the beam power was deposited in the target station and 5 % is thought to be absorbed as binding energy or escape the system. For both proton energies, the total power deposited in the target was found to be about 55 % of the proton beam power.

A considerable difference in heat deposition between 2.2 and 9.0 GeV protons is noticed in the moderators and shield. Since the volume of the first target moderators are a half of the flux trap or second target moderators, the power density of the moderators are approximately same for 2.2 GeV protons. For 9.0 GeV protons, however, the power density of the first target moderators is about 53 % of the second target moderators. This is because the neutron distribution around the target is more anisotropic and skewed toward the back of the target with higher proton energy. The spatial distribution of the power in moderators has been also investigated because the power density of around 1.5 W/cm^3 for crygenic moderators is significantly high. We have found that about 30 % of heat deposited in water moderators occurs in the 17 % of the moderator volume near the target and at leat 50 % of heat in the moderator can be removed by attaching a premoderator region of 4 cm thickness between the moderator and target.

Table 4 shows a comparison of the results from 2.2 GeV and 9.0 GeV protons. The neutron yield per proton is much higher for 9.0 GeV protons. However, the neutron production rate per MW-beam is higher for 2.2 GeV protons because the target dimension is not adequate to utilize all the energy of 9.0 GeV protons. The neutron leak from the station is higher for 9.0 GeV protons as expected because neutron spectrum is thought to be harder. The maximum power density is lower for 9.0 GeV protons because of longer stopping length of higher energy protons. Thus, higher energy protons penetrates deeper in the target and deposits more energy in the back of the target than lower energy protons. Fig.8 shows a comparison of the axial power distribution in the target between 2.2 and 9.0 GeV protons. It is noticed in Fig.8 that the peak power occurs in the first disk for 2.2 GeV protons but it occurs in the second disk for 9.0 protons. Also, it is observed that the powers in the first target disks are higher for 2.2 GeV protons but the powers in the second target disks are higher for 9.0 GeV protons.

We have further analyzed the power distribution in the reflector and shield as illustrated in Figs. 9 and 10. The volumes of the front and back segments of the reflector are approximately the same while the middle segment is much smaller. Also, the segmentation of the shield are the same as that of the reflector. Hence, it is noticed in Figs.9 and 10 that the heat deposited in the back of both reflectors and shield is much greater than in the front. This is because protons are still energetic even at the end of the target in addition to the anisotropic distribution of neutrons as discussed earlier. The anisotropic power distribution in the reflector and shield is more significant with 9.0 GeV protons, for instance, the power in the back half of the shield is seven times larger than the power in the front half of the shield. This spatial distribution of heat load in the surroundings of the target is though to bring a special attention not only to the cooling system design but also to the radiation protection consideration because higher heat load indicates higher radiation dose also. For the heat load in the back of the shield, the heat deposited by high energy particles (i.e., heat load calculated by LAHET) was 1.5 time higher than that deposited by low energy neutrons (i.e., heat load calculated by MCNP) for 2.2 GeV protons. The ratio of the two heat depositions was 2.07 for 9.0 GeV protons. The statistical uncertainty of the calculation is less than 3 % for the target power and maximum 10 % for the individual moderator powers.

Table 3 Heat deposition in the target station per MW proton beam

Component	Heat Deposition (kW) by 2.2 GeV protons	Heat Deposition (kW) by 9 GeV protons
Target	550.8 (total)	553.6 (total)
1st target	306.5	251.0
2nd target	244.3	302.6
Coolant	21.0	14.5
Housing	34.2	40.0
Moderator Total	7.6 (total)	6.4 (total)
1st top moderator	0.775	0.413
1st bottom moderator	0.773	0.417
flux trap moderator - right	1.516	1.30
flux trap moderator - left	1.498	1.27
2nd top moderator	1.582	1.54
2nd bottom moderator	1.477	1.50
Boron Decoupler	26.7	20.1
Reflector	126.6	120.4
Shield	128.0	187.0
Removable Assembly	7.0	6.6
Target Station Total	901.9	948.6

Table 4 A comparison of key results between 2.2 and 9.0 GeV protons

Proton energy	Neutron yield per proton	Neutron production rate per MW-beam	Maximum power density [a] (kW/cm^3)per MW-beam	Neutron leak per proton
2.2 GeV	49.3	1.40×10^{17} n/sec	1.650 at 1st disk	9.67
9.0 GeV	151.5	1.05×10^{17} n/sec	1.216 at 2nd disk	38.83

[a] the power density at the center with r = 1 cm

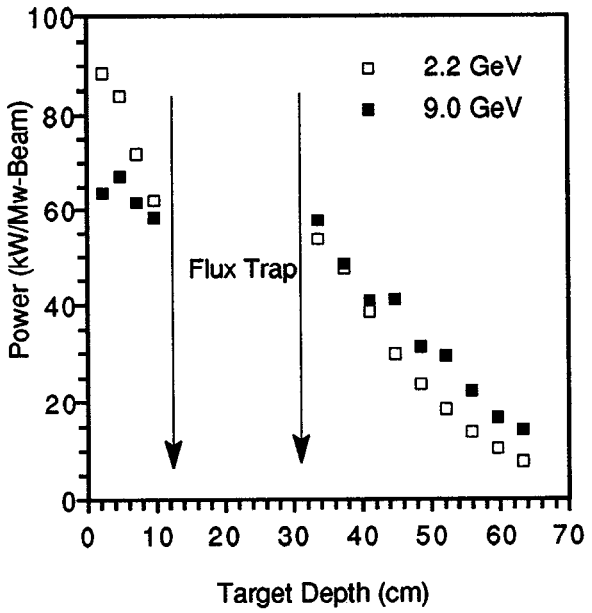

Fig.8 Axial power distribution along the target

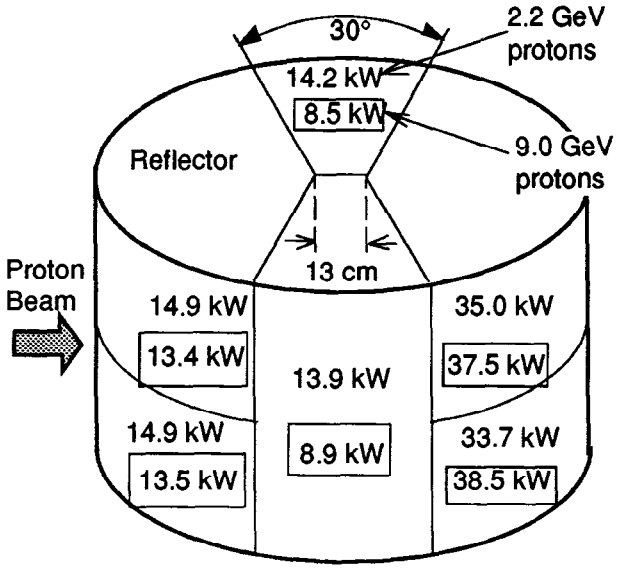

Fig.9 Power distribution in the reflector

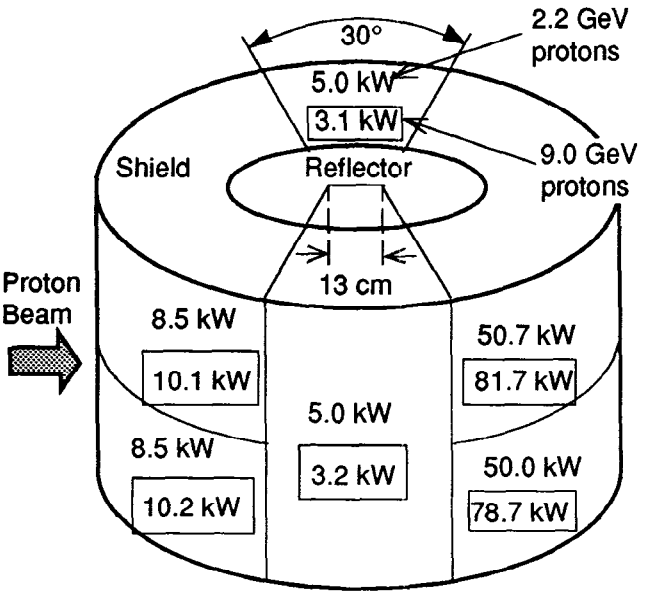

Fig.10 Power distribution in the shield

4. Neuron Beam Characteristics

In Fig.11 the neutron current spectra outgoing from the surface of the moderators are compared for the case of 2.2 GeV protons. It is seen in Fig.11 that the shape of neutron spectrum is almost same for all six moderators and that the 1st moderators result in the highest neutron current in all energy bins. Fig. 12 shows the neutron spectra at the end of the center beam lines from the 1st target, flux-trap, and 2nd target moderators. At the end of beam lines, the neutron beam from the flux-trap moderator is slightly higher than those from the other two moderators especially for the thermal energy region. The change of the neutron beam spectrum along the beam line from the moderator surface to the end of beam line is shown in Fig.13 The neutron beam intensity becomes smaller as it approaches the end of beam line over the entire range of neutron energy as expected. However, the ratio of thermal to fast neutrons decreases most significantly in the decoupling region which is between the moderator to the end of decoupler. The decoupler cuts off the thermal neutrons coming into the beam line from the reflector while it is transparent to fast neutrons. The total number of neutrons produced in the target is 49 neutrons per proton with 2.2 GeV protons. The total number of neutrons available at the end of beam lines which are about 85 ~ 90 cm away from the moderator surface is found to be 0.62 per proton.

The comparisons of neutron beam characteristics between 2.2 and 9.0 GeV protons are shown in Figs.14 through 16. A noticeable effect of higher proton energy is that the neutron distribution around the target is more skewed toward the back of the target, i.e., the tangential angle of the neutron velocity to the proton beam direction is smaller in addition to the increase of the neutron generation in the back of the target with higher energy protons. Thus, more neutrons are concentrated in the back region of the target. As seen in Figs. 14 and 15, the neutron spectra from the first target and flux trap moderators are smaller for 9.0 GeV protons than 2.2 GeV protons while those from the second target moderators are almost the same. The shape of neutron spectra from all moderators are almost identical regardless of impinging proton energies. This is thought to indicate that the volume of moderators used in the calculation is adequate to attain an equilibrium spectrum regardless of the source neutron spectrum generated in the target.

The statistical errors of the Monte Carlo calculations are less than 7 % for the neutron beams at moderators for all energy bins. Because of small population of neutrons at the end of beam lines, the statistical uncertainty at the end of beam lines is relatively large. Thus, the error ranges are indicated in Fig.11.

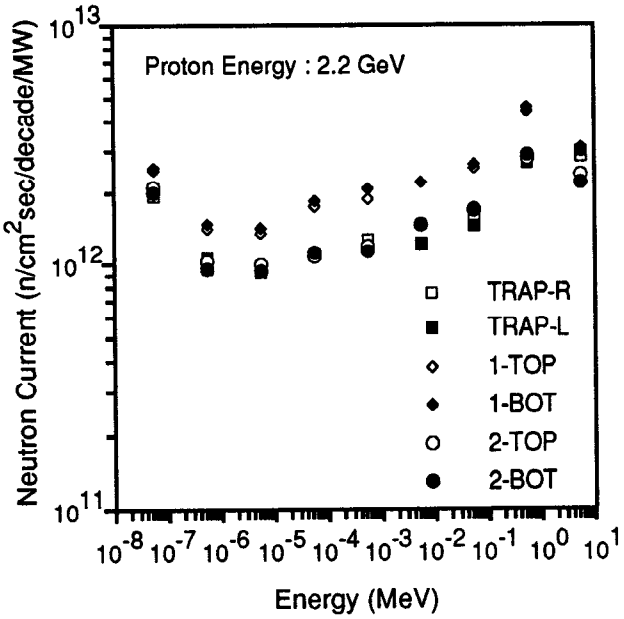

Fig.11 Neutron beam spectra at the moderator surfaces

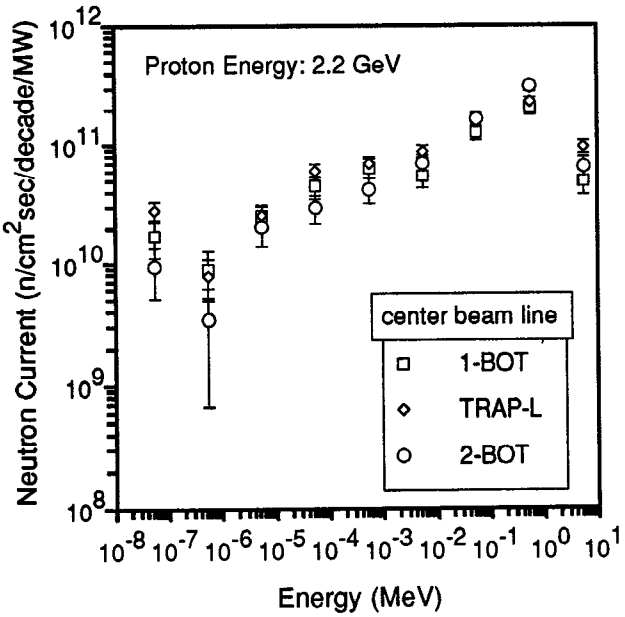

Fig.12 Neutron beam spectra at the end of beam lines

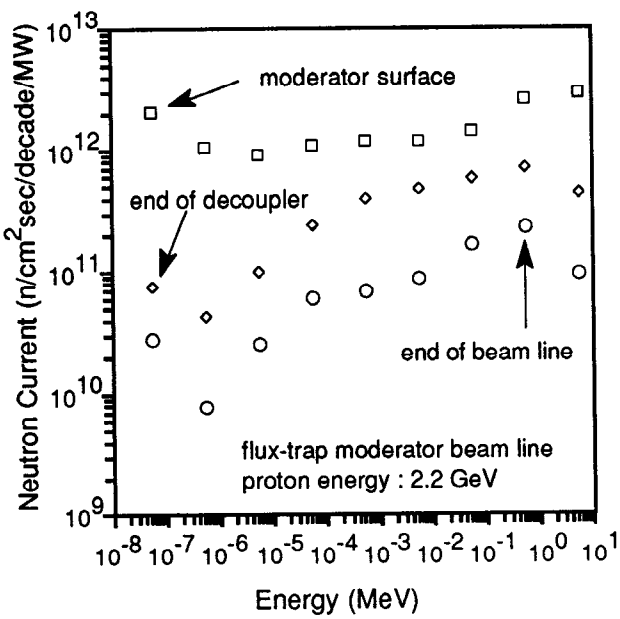

Fig.13 Change of neutron beam spectrum along the beam line

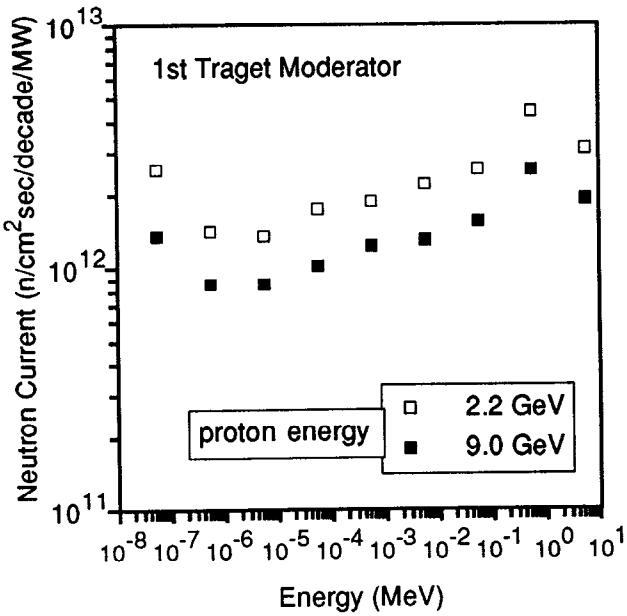

Fig.14 Effect of proton energy on neutron beam from the 1st target moderator

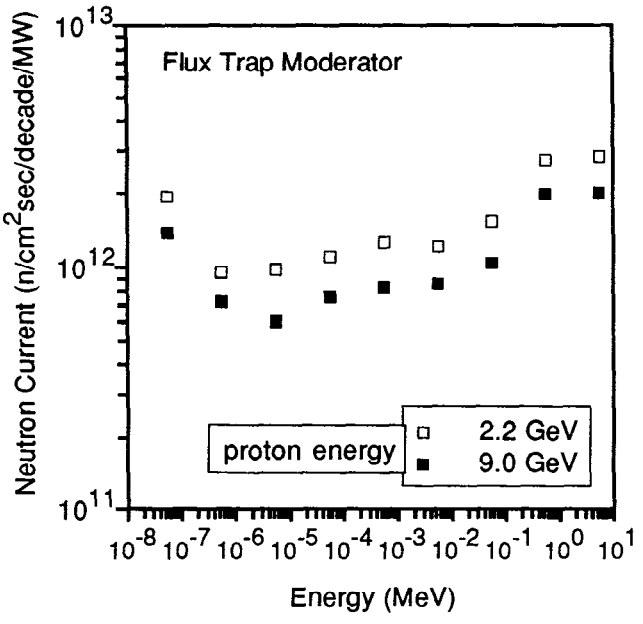

Fig.15 Effect of proton energy on neutron beam from the flux trap moderator

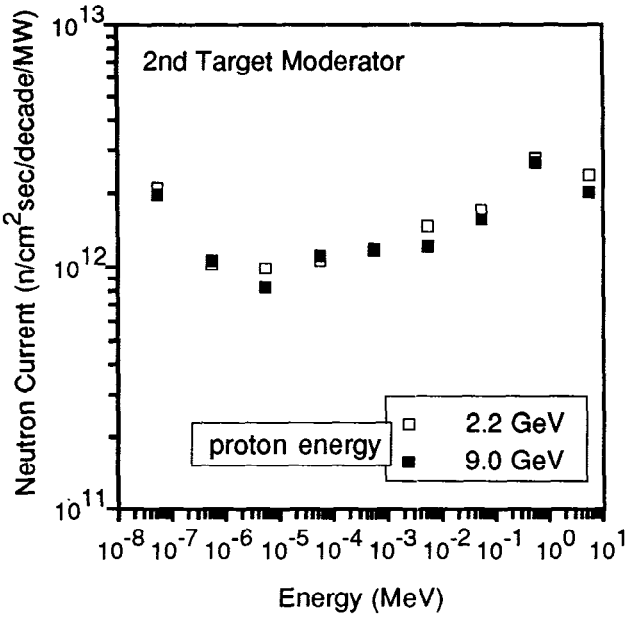

Fig.16 Effect of proton energy on neutron beam from the 2nd target moderator

5. Conclusions

We have investigated the effect of proton energy on the heat load and neutron yield in the target. The results have shown that the higher proton energy offers an advantage in target cooling because the peak power density is lower. However, the neutron production rate and maximum neutron current at a given proton beam power was observed to be reduced if proton energy is higher than 1.5 GeV. The total power deposited in the target was found to be insensitive to proton energy. The ratio of the target heat load to proton beam power was approximately 0.6 to 0.7 if the target dimension is sufficiently large to accomodate proton beam and cascade process. With a realistic target model under the current study, this conclusion of the target heat load was observed as well. However, for the power distribution in the surrounding system, i.e., reflector and shield, a large difference of heat load in space was found. The heat load was much higher in the back of the target station than in the front. Thus, the cooling of the surroundings needs to take account of the spatial variation of heat load. The neutron beam spectrum from moderators in the realistic target model did not change significantly with different proton energies. However, the spatial distribution of neutron beam was found to vary significantly according to the proton energy, i.e., higher proton energy resulted in lower neutron beam intensity from the moderators installed at the front of the target.

REFERENCES

1. Richard E. Prael and Henry Lichtenstein, " User Guide to LCS: the LAHET Code System", LA-UR-89-3014, Los Alamos National Laboratory, Sept. 1989.
2. T. W. Armstrong et al, "Theoretical Target Physics Studies for the SNQ Spallation Neutron Source", Jul-Spez-120, KfK Karlsruhe, Germany, July 1981.
3. N. Watanabe et al, "Report of the Moderator Working Group", International Workshop on the Technology of Targets and Moderators for Medium to High Power Spallation Neutron Sources, Paul Scherrer Institute, Switzerland, Feb. 1992.